



**HAL**  
open science

# Immobilisation of contaminants by ‘green’-synthesized magnetite as a remediation approach to the phosphogypsum waste leachates model solution

Evgenia-Maria Papaslioti, Philippe Le Bouteiller, Hugo Carreira, Jean-Marc Greneche, Alejandro Fernandez-Martinez, Laurent Charlet

## ► To cite this version:

Evgenia-Maria Papaslioti, Philippe Le Bouteiller, Hugo Carreira, Jean-Marc Greneche, Alejandro Fernandez-Martinez, et al.. Immobilisation of contaminants by ‘green’-synthesized magnetite as a remediation approach to the phosphogypsum waste leachates model solution. *Journal of Environmental Management*, 2023, 341 (2), pp.117997. 10.1016/j.jenvman.2023.117997 . hal-04235238

**HAL Id: hal-04235238**

**<https://hal.science/hal-04235238>**

Submitted on 10 Oct 2023

**HAL** is a multi-disciplinary open access archive for the deposit and dissemination of scientific research documents, whether they are published or not. The documents may come from teaching and research institutions in France or abroad, or from public or private research centers.

L’archive ouverte pluridisciplinaire **HAL**, est destinée au dépôt et à la diffusion de documents scientifiques de niveau recherche, publiés ou non, émanant des établissements d’enseignement et de recherche français ou étrangers, des laboratoires publics ou privés.

# **Immobilisation of contaminants by ‘green’-synthesized magnetite as a remediation approach for the phosphogypsum waste leachates**

**Evgenia-Maria Papaslioti<sup>1\*</sup>, Philippe Le Bouteiller<sup>2</sup>, Hugo Carreira<sup>1</sup>, Alejandro Fernandez-Martinez<sup>1</sup>, Laurent Charlet<sup>1</sup>**

<sup>1</sup>Univ. Grenoble-Alpes, Univ. Savoie Mont Blanc, CNRS, IRD, Univ. Gustave Eiffel, ISTerre, 38000, Grenoble, France

<sup>2</sup>HYMAG'IN, Grenoble, France

\*evgenia-maria.papaslioti@univ-grenoble-alpes.fr

**Keywords:** Magnetite; Phosphogypsum; Arsenic; Antimony; Uranium; (Nano) Zero-Valent Iron; Vivianite; Remediation technique

**To be submitted to: Journal of Hazardous Materials**

## **Abstract**

The removal of arsenic, antimony and uranium by magnetite from contaminated waters is a promising technology. In the present experimental study, a magnetite recycled from the steel industry was used to investigate the sorption of those contaminants in phosphate-free, and phosphate-rich suspensions, searching for an efficient remediation for the acidic phosphogypsum leachates derived from the phosphate fertilizer industry. The results showed up to 98% U removal under controlled pH conditions, while phosphate did not hinder this immobilization. In contrast, the results confirmed the limited uptake of As and Sb oxyanions by magnetite in presence of a competing anion such as phosphate, displaying only 7-11% removal, compared to 83-87% in the phosphate-free sorption experiments. (Nano) Zero-Valent Iron anaerobic oxidation was examined as mechanism to increase the pH and as a source of Fe<sup>2+</sup> with the aim to remove phosphate via vivianite precipitation, prior to the reaction with magnetite. UV-Vis, XRD and SEM-EDS showed that vivianite precipitation occurs at pH>4.5, mainly depending on the phosphate concentration; the higher the [PO<sub>4</sub><sup>3-</sup>], the lower the pH at which vivianite precipitates. It is anticipated that an optimum design with separate reactors controlling the conditions of NZVI oxidation, followed by vivianite precipitation and finally, reaction with magnetite, can achieve high contaminant uptake in field applications.

## 1. Introduction

### 1.1 Reduction of contaminants by magnetite

The problematic of drinking and waste water contamination by various inorganic toxic pollutants has gained a worldwide attention and the scientific community has greatly focused on finding innovative decontamination techniques. The ubiquitous presence of iron (hydr)oxides and their redox transformations control the mobility of various redox sensitive elements, nutrients and radionuclides in the environment and in engineered systems (**Schwertmann and Taylor, 1989**). These solids have the greatest adsorption capacity per unit mass among environmentally-relevant solid phases (**Missana et al., 2009**), and their ability to retain metals and metalloids on their surface is an important factor of the immobilisation of contaminants. Controlled experimental systems mimicking in-situ conditions are necessary to study the geochemical processes controlling Fe transformation and subsequent contaminant retention or release. While the immobilisation of contaminants by various Fe (hydr)oxides (e.g. ferrihydrite, hematite) has been broadly investigated, retention by magnetite is far less documented. Magnetite ( $\text{Fe}_3\text{O}_4$ ) is an iron oxide containing both  $\text{Fe}^{2+}$  and  $\text{Fe}^{3+}$  ions, and it has been suggested to be a significant reductant for contaminants due to its ubiquity in the environment (**Gorski et al., 2009**). (Nano)magnetite has a high specific surface area and, when exposed to acidic conditions, it is transformed to maghemite, releasing  $\text{Fe}^{2+}$ , which induces the reductive precipitation of inorganic contaminants (Poulain et al., 2022) or the transformation of organic contaminants (**Gorski et al., 2009**). Magnetite has been reported to be efficient in immobilising various inorganic contaminants, such as Cr (**He et al., 2005**), As (**Zhang et al., 2010**), U (**Scott et al., 2005; Crane et al., 2011; Pan et al. 2020**), Se (**Martinez et al., 2006; Missana et al., 2009**), and Sb (**Kirsch et al., 2008**). The use of (nano)magnetite is becoming an emerging technology for the treatment of contaminated land and water with a great potential to become an effective and low-cost alternative to conventional remediation techniques. Also, while the retention of contaminants by iron-bearing minerals in presence of microbial activity is well documented, the reactivity under abiotic and acidic conditions has been less documented.

Magnetite can be produced from the waste products of steel industry (**Crouzet et al., 2017**). Here, as an alternative idea for the removal of contaminants, we took advantage of this circular economy concept to exploit an existing and increasingly produced waste as a source of material to decontaminate industrial effluents. Among all the wastes produced by the steel industry, the

one that corresponds to the very fine powder ( $< 1\text{mm}$ ) is less easy to reuse or recycle. HYMAG'IN, a start-up company from the University of Grenoble-Alpes, develops a process for the transformation of this waste into magnetite, planning to produce a few thousand tons of magnetite/year/industrial site (Brunet et al., 2017). This patented technology is based on a soft chemical dissolution/precipitation process called hydrothermal oxidation. The process is entirely based on reactions with water, and does not require any volatile or organic solvent, strong acid or flammable gas, fitting well with the 'Green chemistry' paradigm. The HYMAG'IN process produces various types of magnetite powders with size ranging from 100 nanometer to a few micrometers. Depending on the iron content of the incoming waste, some impurities may be found in the end product, such as fayalite, rutile or corundum minerals, with molar ratios from 0% to 20%. Here, we used one sample of magnetite produced by the HYMAG'IN process for our experiments.

## 1.2 Environmental implications of the phosphogypsum waste

Phosphogypsum (PG) is the main waste generated by the phosphate fertilizer industry, and is produced by the wet chemical digestion of phosphate ore (fluorapatite,  $\text{Ca}_5(\text{PO}_4)_3\text{F}$ ) by sulphuric acid ( $\text{H}_2\text{SO}_4$ ) to generate phosphoric acid ( $\text{H}_3\text{PO}_4$ ). PG is a hazardous material that threatens the environment welfare worldwide. For every ton of phosphoric acid manufactured, 5 tons of PG are generated, and its worldwide production has reached 100–280 Mt per year (Yang et al., 2009; Macias et al., 2017). PG leachates are characterised by an extreme acidity, with pH values ranging from 1.8 to 4.8 (as in the Huelva PG stacks, Spain; e.g. Pérez-López et al., 2016; Papaslioti et al., 2018a), and by the high content in radioactive and toxic elements due to their presence in the original phosphate ore and their occurrence of residual phosphoric acid, in addition to other chemical reagents, such as sulphuric and hydrofluoric acids, ammonium hydroxide or amine (Lottermoser, 2010). These impurities strongly limit the potential reuse of phosphogypsum, e.g. as a construction material (Cánovas et al., 2018). PG wastes are usually stockpiled in coastal areas close to phosphate fertilizer plants, where they are exposed to weathering conditions (Tayibi et al., 2009). They are a significant source of environmental contamination under leaching (Lottermoser, 2010; Pérez-López et al., 2016). Despite the high level of pollutants found in phosphogypsum and the stacks proximity to cities, there are no specific regulations for the management of this waste (Macias et al., 2017).

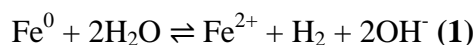
Some of the most problematic contaminants contained in the PG acidic effluents are the redox sensitive As, Sb and U elements. Arsenic is a toxic trace element, whose fate and bioavailability strongly depends on its speciation. Arsenic-contaminated drinking water has been a severe problem in many areas worldwide (Yean et al., 2005; Charlet and Polya, 2006), and the health hazard due to the chronic exposure to arsenic is well established (e.g. Tseng et al., 1968; Anderson and Bruland, 1991). Similarly, antimony (Sb) is a toxic, geogenic and anthropogenic metalloid, ubiquitously present in the environment, and considered as a priority pollutant by the United States Environmental Protection Agency (USEPA) and EU (Filella et al., 2002). Excess Sb intake by humans may cause, like As, various toxicity related health problems (Wilson et al., 2010; Boreiko and Rossman 2020). Thus, the focus of research has now shifted to develop treatment methods using suitable sorbents to achieve low As and Sb levels in drinking water. Both oxyanions are present in PG leachates at significant levels, e.g. up to 45 and 0.3 mg/L, respectively (Papaslioti et al., 2018a), and are the most problematic PG drainage water contamination concerns. Their immobilisation is hindered by the presence of high phosphate levels (i.e. >2500 mg/L), as phosphate competes with As and Sb oxyanions for sorption sites. Though only 15% of U present in the phosphate rock remains in the PG waste (Abril et al., 2009), its concentration is still too high for the solid to be used in a recycling process. For instance, values reported for total U in the huge PG stack present in Huelva (Spain) are in the 0.5 to 19 mg/L range (Papaslioti et al., 2018a).

In search for an efficient remediation technique for the PG stacks, some treatment systems have been tested. For example, the feasibility of an alkaline treatment system by the addition of a  $\text{Ca}(\text{OH})_2$  solution to the PG acidic leachates has been studied for a PG located in an estuarine environment degraded by such pollution (Millán-Becerro et al., 2019). High removal values were reached for most contaminants, but the system was not significantly effective for As and Sb removal. In addition, large amounts of contaminant-rich lime waste products produced by such industrial process, due to the extreme acidity of the treated leachates, would have to be stored. Another research approach introduced the induction of controlled redox oscillations in the same PG system in order to mimic the fluctuation of water saturation and redox conditions, caused either by the tidal flood or by monsoon (Papaslioti et al., 2020), controlling the behaviour of dominant redox sensitive species (i.e. Fe and S). A negligible effect of the redox oscillations was observed on the studied pollutants (Zn, As, Cd, U, and Sb) compared to the effect in low

phosphate synthesis (Parsons et al., 2013), inducing poor adsorption to Fe (hydr)oxides due to high phosphate concentration and very low pH conditions, in addition to limited sulphide precipitation, due to the short induced redox cycles.

### 1.3 Precipitation of phosphate-Fe vivianite mineral

As indicated by previous studies (Millán-Becerro et al., 2019; Papaslioti et al., 2020), the presence of phosphate in waste leachates hinders the removal of As and Sb oxyanions. Many potential phosphate removal mechanisms are Fe-based, including adsorption, precipitation and coprecipitation. For instance, vivianite ( $\text{Fe}_3(\text{PO}_4)_2 \cdot 8\text{H}_2\text{O}$ ) precipitation is an emerging technology for phosphate immobilisation and P recovery due to its natural ubiquity, foreseeable economic value (e.g. Liu et al., 2018; Cao et al., 2019; Wu et al., 2019; Liu et al., 2021). Vivianite is a commonly identified mineral in many natural and aquatic systems. It is an important sink for dissolved  $\text{Fe}^{2+}$  in phosphate rich environments, due to its thermodynamic stability ( $K_{\text{sp}} = 10^{-36}$ ), and is thus easily precipitated (Miot et al., 2009; Liu et al., 2021). It has various industrial applications, in the manufacturing of secondary Li-ion batteries and slow-released fertilizer (Cao et al., 2019; Wu et al., 2019). In addition, vivianite has been identified as a dominant phase in experiments performed in PG geochemistry studies and remediation approaches (Papaslioti et al., 2018b; Papaslioti et al., 2020). Another Fe-based reducing agent is the (nanoscale) zero-valent iron (NZVI), which is commonly used to treat contaminated waters (e.g. Kanel et al., 2005; Bae and Hanna, 2015; Almeelbi and Bezbaruah, 2012). It is highly reactive, abundant and cheap, and has an extremely large surface area (Choe et al., 2000; Kanel et al., 2005; Liu and Wang, 2019). It can be in in-situ large-scale groundwater treatment units as it can be transported effectively through aquifers due to its small size and its capacity to remain in suspension (Zhang et al., 2003; Kanel et al., 2005). In the present study, NZVI is examined as a source of  $\text{Fe}^{2+}$  for vivianite formation, and at the same time as a pH buffer due to its anaerobic oxidation (corrosion) as shown in Eq. 1:



This  $\text{Fe}^{2+}$  aqueous ion production may induce vivianite precipitation (Eq. 2) thus, acting as a potential phosphate removal pathway for acidic waste leachates:



The aim of the present study is to fulfil some of the existing knowledge gaps on contaminant sorption by magnetite and to suggest management techniques for the remediation of toxic, acidic, and phosphate rich PG wastes, as well as other phosphate-rich wastes (e.g. waste activated sludge; **Cao et al., 2019**). We address the combined interactions of physical and geochemical processes regulating the fate of most redox sensitive elements, in a controlled but complex setting, representative of natural systems. This research focuses on the effect of magnetite on (i) U reduction thus reducing the threat posed by PG waste radioactivity worldwide and (ii) As and Sb oxyanion removal, thus on a reduction of As and Sb toxicity and raising levels of population impregnation due to the ineffectiveness of the current PG remediation strategies up to date. The optimum parameters for vivianite precipitation are investigated as an early phosphate removal step from PG waste effluents, prior to magnetite interaction, as described above. The purpose of the present research is to set the basis of an industrial process to decontaminate PG effluent waters through (i) the use of ZVI (here scaled down by the use of NZVI) to increase the pH of the water while producing  $\text{Fe}^{2+}$ , with (ii) precipitation of phosphate ions as vivianite, and (iii) the use of magnetite derived from steel industry wastes to immobilize toxic pollutants under different pH conditions and high phosphate concentrations. This three-step process provides new insights into a new 'green' route for the decontamination of drinking and wastewaters.

## **2. Materials and methods**

### **2.1 Materials and chemicals**

HYMAG'IN magnetite with a purity of 87% was used for the experiments. XRD analysis show the presence of two other mineral phases: rutile (10%), and elemental iron (3%) which has not been fully dissolved and oxidized during the process. SEM particle measurement reveals a median size of 377 nm. The surface area of the solid was determined by the BET method and a value of  $12 \text{ m}^2/\text{g} \pm 3\%$  was obtained. All chemicals used for synthesis and stock solutions, ( $\text{FeCl}_3 \cdot 6\text{H}_2\text{O}$ ,  $\text{NaBH}_4$ ,  $\text{FeCl}_2 \cdot 4\text{H}_2\text{O}$ ,  $\text{NaH}_2\text{PO}_4$ ,  $\text{NaCl}$ ), are analytical reagents, purchased from Sigma-Aldrich. ICP-standards solutions of 1g/L were used as  $\text{As}^{+5}$ ,  $\text{Sb}^{+5}$ , and  $\text{U}^{+6}$  source. Reagent grade NaOH ( $\geq 98\%$ , Sigma Aldrich) and HCl (37 %, Carl Roth) were used for preparation of 1 M and 0.1 M stock solutions for pH control. The synthesis of necessary products and all the experiments, apart from the sorption ones, were conducted at room temperature inside a Jacomex glove box, filled with Ar, with a controlled oxygen partial pressure maintained below 2 ppm,

using boiled and argon-degassed Milli-Q water (18.2 M $\Omega$ ·cm) for all the solutions and suspensions.

## 2.2 Sorption experiments

A magnetite suspension of 2 g/L was prepared by mixing the solid with a NaCl solution of Ionic Strength (IC) = 0.1 M, mimicking the IC of the phosphogypsum waste waters. All experiments were conducted in serum bottles (200 mL) and were kept under continuous stirring for homogenization of the suspension. Short term kinetic batch experiments were conducted of 4 hrs each, at different pH values (2.5, 5, and 7) for comparison, using HCl and NaOH solutions for pH adjustment. Aliquotes were collected at different time intervals after pH adjustment and monitoring before each sampling using a Metrohm 781 pH Meter. They were filtered using 0.22  $\mu$ m filters. All aliquotes were acidified with 1% supra-pure nitric acid to keep the analytes of interest in solution, and were stored at 4 °C. A first experiment was performed to observe the kinetics of magnetite dissolution at the three different pH values, with no contaminants added. Next, U adsorption by magnetite was studied by adding 0.0076 mM of U at the magnetite suspension at  $t = 120$  min. The synergetic effect of As (0.04mM), U (0.0076 mM) and Sb (0.002mM) was tested separately at the same conditions. The same experiments were repeated using a mixture of NaCl and NaH<sub>2</sub>PO<sub>4</sub> as the solution matrix, keeping the IC = 0.1 M, with the aim of studying contaminant adsorption under high phosphate concentration (26.46 mM). Another series of sorption experiments was conducted, by reacting natural PG wastewater with magnetite at pH ~2.5 (real conditions) and, after adjusting the pH at ~5.5.

## 2.3 NZVI oxidation experiments as a function of pH

The NZVI material was synthesized by dropwise addition of a 1.6 M NaBH<sub>4</sub> aqueous solution to a 1 M FeCl<sub>3</sub>·6H<sub>2</sub>O aqueous solution under magnetic stirring, as described by **Wang and Zhang (1997)**, and **Kanel et al. (2005)**. In order to study the pH dependent oxidation rate of NZVI, kinetic experiments were performed under anoxic conditions by reacting 0.2 g/L of the synthesised NZVI with pure water at different starting pH values (2.5, 4, 5, 6, and 7). Experiments were performed for up to 5 hrs each, monitoring the pH and the Fe<sup>2+</sup> concentration regularly. Based on the results, further oxidation experiments were conducted for 60 min each, by reacting NZVI (0.1 and 0.2 g/L) with pure water of pH 2.5 (value of the PG waste acidic leachates).

## 2.4 Vivianite precipitation experiments

With the aim of finding the optimal conditions for the nucleation of vivianite, various kinetic experiments were conducted, combining different  $\text{Fe}^{2+}/\text{PO}_4^{3-}$  molar ratios, at different phosphate concentrations (5, 10, 15, and 25 mM) (**Table 1**). The duration of each experiment was 60 min and samples were collected regularly to follow the behaviour of  $\text{Fe}^{2+}$  and  $\text{PO}_4^{3-}$  in solution, while monitoring the evolution of pH. The analytical reagents used for the preparation of the  $\text{Fe}^{2+}$  and  $\text{PO}_4^{3-}$  stock solutions were  $\text{FeCl}_2 \cdot 4\text{H}_2\text{O}$  and  $\text{NaH}_2\text{PO}_4$ , respectively. Solid samples were collected (when reaction occurred) at the end of the experiments (at  $t = 60$  min) to characterize the precipitates.

**Table 1:** Conditions of the vivianite precipitation experiments:  $[\text{PO}_4^{3-}]$  at  $t=0$  and at  $t = 5$  min; Fe/P molar ratio, initial and final pH, total [Fe] at  $t=5$  min, %  $[\text{PO}_4^{3-}]$  removal and SI of vivianite calculated by PHREEQC at the given parameters.

$\text{PO}_4^{3-}$ (mM); $t = 0$	Fe/P molar ratio	$\text{pH}_{\text{initial}}$	SI vivianite	$\text{PO}_4^{3-}$ (mM); $t = 5$ min	Fe (mM); $t = 5$ min	$\text{pH}_{\text{final}}$	% $[\text{PO}_4^{3-}]$ removal
25	0.5	6.16	10.44	13.98	0.341	5.66	44.08
25	1	5.28	10.98	15.65	7.442	4.01	37.40
25	1.5	4.95	11.22	22.07	29.80	3.83	11.72
15	0.5	6.05	9.71	13.30	0.363	5.57	11.33
15	1	5.25	10.16	12.02	6.559	4.12	19.87
15	1.5	4.85	10.35	10.75	14.08	3.96	28.33
10	0.5	5.44	7.78	8.521	2.560	4.47	14.79
10	1	5.27	8.1	8.260	6.977	4.24	17.40
10	1.5	5.11	8.21	8.345	10.59	4.20	16.55
5	0.5	6.17	7.31	4.012	0.990	4.99	19.76
5	1	6.10	7.6	4.030	3.389	4.57	19.40
5	1.5	5.90	7.5	4.092	4.058	4.52	18.16

## 2.5 Analytical methods

### 2.5.1 Solution analysis

Elemental concentrations were determined via Inductively Coupled Plasma-Optical Emission Spectrometer (ICP-OES) using a Varian 720-ES instrument at the Institute of Earth Sciences (ISTerre) in Grenoble (France). Detection limits in  $\mu\text{g/L}$  were 0.12 for Fe, 2.1 for P, 1.5 for As, 2 for Sb, and 3 for U. Iron, P, As, Sb, and U ICP-standard solutions of 1 g/L were prepared with the same matrix as the samples and were analysed by ICP-OES as external standards. Dilutions were performed to ensure that the concentration of the samples was within the concentration range of instrument calibration and blank solutions with the same matrix as the samples were also analysed. The average measurement error was below 5% for all analyses.

### **2.5.2 Nucleation of vivianite**

Solutions prepared with the same parameters used for the kinetic experiments of vivianite formation (see paragraph 2.4) were prepared additionally for analysis by UV-Vis, in order to determine the induction time and follow the rate of vivianite nucleation. The mixing of the solutions was performed directly before measurement by a Cary 3500 UV-VIS Spectrometer, which is used to determine changes in the absorbance of the solution and hence correlate it with the kinetics of formation of a phase in the solution. A blank solution was prepared with 2 mL of MilliQ water. Each solution was put in plastic square cuvette (12.5\*12.5\*45 mm). Each experiment was conducted for over 1 hour at a fixed temperature of 25°C, with a stirring of 800 revolutions per minute (using a magnetic bar of 7 mm long and 1 mm wide). The absorbance of the solution over time was determined using a wavelength of 500 nm, a spectral bandwidth of 5 nm, and a collection time of 1 s.

### **2.5.3 Solid analysis**

**XRD.** The original magnetite, the solid material collected after each sorption experiment, and the solid material collected after each vivianite precipitation experiment were analysed using X-ray diffraction (XRD) analysis with a Bruker D8 diffractometer with Cu radiation ( $\lambda = 1.54 \text{ \AA}$ ) and Vortex-EX detector (Hitachi), showing no distinct impurity diffraction peak, after prepared on a silicon plate and sealed in the air-tight powder holder.

**BET.** The specific surface area (SSA) was determined by the Brunauer–Emmett–Teller adsorption method (BET- $\text{N}_2$ ) at 77 K, using a Belsorp-Max (Bel Japan) volumetric gas sorption instrument. A small amount (0.418 g) of magnetite was loaded in a glass cell inside the glovebox

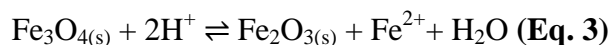
and then dried under vacuum at 80 ° C during 12 h. The SSA was calculated from the BET equation in the  $P/P_0$  range 0.052-0.307.

**SEM-EDS.** The solid material collected after each vivianite-precipitation experiment was prepared for analysis by Scanning Electron Microscopy (SEM). Powder samples were put on pins, previously covered by a self-adhesive carbon film, and then coated with 1 nm of Au using a Cressington Sputter Coater 108 Auto. Samples were analysed by a Tescan Vega 3 SEM, collecting images by Secondary (SE) and Backscattered Electrons (BSE) at 16 keV.

### 3. Results

#### 3.1 Uranium sorption by magnetite

At neutral pH, zero to minimal magnetite dissolution occurred throughout the experiment, as previously reported (**Poulain et al., 2022**). A very fast adsorption of U by magnetite was observed, reaching up to 98% removal efficiency only 10 min after the addition of U in the magnetite suspension (at  $t=130$  min of the experiment; **Fig. 1C**). The remaining U concentration in solution was thereafter stable, with no further sorption or desorption from magnetite until  $t = 240$  min. At lower pH, magnetite surface layer is transferred to maghemite via **Eq. 3**.



So, in contrast with neutral pH, at pH 5 magnetite transformation to maghemite was very fast (only after 30 min). Right after U addition to the suspension, the concentration of Fe in solution was doubled and then it was stable until the end of the experiment (**Fig. 1A**). However, the increase of Fe in solution ( $\sim 0.3$  mM) is much larger than the decrease of U, ( $\sim 6.5$   $\mu\text{M}$  sorbed) (**Table S1**), so it cannot be explained by an  $\text{UO}_2^{2+}/\text{Fe}^{2+}$  simple cation exchange mechanism at the surface of magnetite. Uranium concentration in solution decreased rapidly (67% removal after 30 min of magnetite reaction with U at pH 5), followed by a slower, but steady sorption, reaching an 88% decrease after 120 min of reaction (at  $t = 240$  min of the experiment; **Fig. 1C**), unlike the experiments at pH 2.5, in which U behaved conservatively, i.e. is mainly not sorbed at all. More specifically, U is exhibiting a poor sorption to magnetite (but a 12% maximum), followed by a fast desorption (**Fig. 1C**). In these very highly acidic conditions, the adsorbent continues to dissolve according to Eq. 3 at a high rate, with a steadily increase of  $\text{Fe}^{2+}$  concentration through the experiment (**Fig. 1A**).

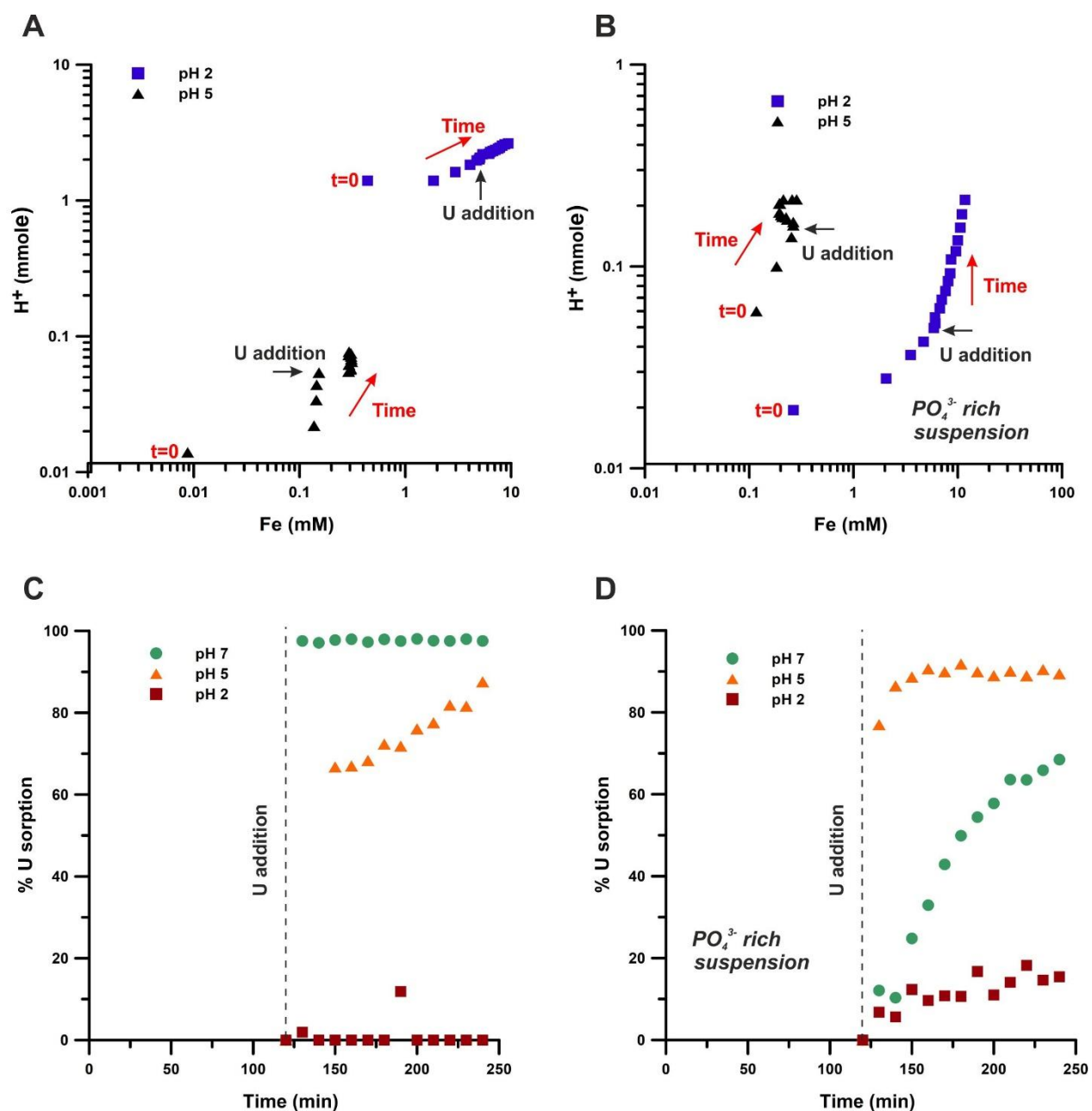


**Figure 1:** Magnetite dissolution (A and B), and U removal (C and D) through time. **A:**  $Fe^{2+}$  released as a function of cumulated added  $H^+$  (log scale) to keep the pH at a value of 2 (blue square) or 5 (black triangle), in absence of phosphate; **B:**  $Fe^{2+}$  released as a function of cumulated added  $H^+$  (log scale) to keep the pH at a value of 2 (blue square) or 5 (black triangle), in presence of phosphate (26 mM); **C:** % U removal in absence of phosphate at pH 2 (red square), 5 (orange triangle), and 7 (green circle); **D:** % U removal in presence of phosphate (26 mM) at pH 2, 5, and 7. [U] added in suspensions is equal to 7.6  $\mu$ M. Uranium was added in all suspensions at  $t = 120$  min.

### 3.2 U sorption by magnetite in phosphate presence

In the presence of phosphate, at neutral pH conditions, we observed a slow deprotonation and limited magnetite dissolution. A slow, kinetically controlled reaction prevailed, achieving up to 68% uranium removal from solution after 120 min of reaction with magnetite at pH 7 (**Fig. 1D**), which is 30% less compared to the reductive immobilisation in the absence of phosphate. The phosphate removal from solution was very low and could not be shown quantitatively due to very high initial concentrations. However, comparing the absolute concentration values (**Table S1**), the phosphate amount removed from solution (~1-2 mM) was higher than that of U (~6  $\mu\text{M}$ ), so phosphate adsorption to magnetite, and possible competition with many ions for adsorption sites were considered. At pH 5, dissolved Fe in solution increased gradually until  $t = 140$  min, when magnetite dissolution decreased until  $t = 210$  min (**Fig. 1B**). Next, total Fe concentration in solution continued to increase until the end of the sorption experiment at  $t = 240$  min (**Fig. 1B**), while the [Fe] released in solution (~3 mM) was much larger than that of [U] (~6.7  $\mu\text{M}$ ) (**Table S1**), as already shown in the phosphate-free experiments. At pH 5 we observe a very fast U adsorption, with 77% removal from the solution only 10 min after U reaction with magnetite. Up to 91% removal was reached in total, while U concentration in solution almost stabilized after  $t = 140$  min, with no further important sorption or desorption processes (**Fig. 1D**). So, unlike the reaction at neutral conditions, at pH 5 phosphate presence did not appear to hinder U removal by magnetite, despite the fact that the phosphate removed from solution (~3 mM) was also higher than that of U (~6.7  $\mu\text{M}$ ) (**Table S1**). Thus, since U sorption is pH-dependent, the most efficient U removal from solution in a phosphate-rich suspension was observed at pH 5. At pH 2.5, no impact of phosphate was observed on magnetite dissolution, comparing the two experiments (**Figs. 1A & 1B**). However, the decrease of U concentration was limited by the highly acidic conditions in both cases; up to 18% U removal observed at  $t = 240$  min in presence of phosphate, with no further decrease, even with some desorption following (**Fig. 1D**).

### 3.3 Synergetic effect of As, Sb and U sorption by magnetite

The same experiments were conducted with a mixture of As, Sb and U oxyanions to study their synergetic and/or antagonistic effect at pH 5.5 (optimal value for the immobilisation of all three ions). The concentration of Fe released in solution was lower compared to that in the U sorption experiments: ~0.04 mM, and ~0.2 mM in the phosphate-free, and phosphate-rich suspensions, respectively (**Table S2**). Nevertheless, uranium behaviour was not affected in presence of As and

Sb and was fully removed from solution under both phosphate and no-phosphate presence (**Fig. 2**). Without phosphate on magnetite, As and Sb immobilization was up to 87% and 83%, respectively (**Fig. 2A**). On the contrary, phosphate ions compete very efficiently for magnetite adsorption, so the sorption of metalloids was only 7% and 11%, respectively (**Fig. 2B**).

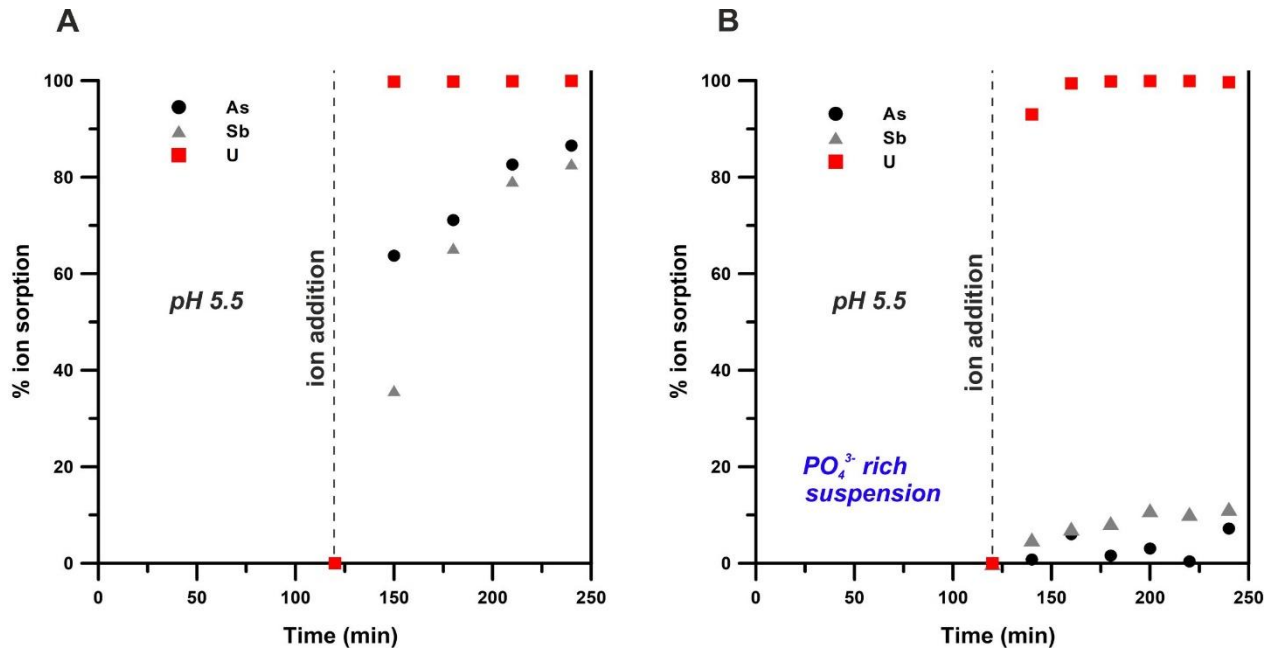


**Figure 2:** Synergetic effect of ions sorption by magnetite through time. **A:** Sorption rate of As (black circle), Sb (grey triangle), and U (red square) without phosphate presence at pH 5.5; **B:** Sorption rate of As, Sb, and U under phosphate presence at pH 5.5.

### 3.4 Effect of magnetite on the acidic phosphogypsum leachates

After observing no effect of magnetite on the contaminants contained in PG wastewater effluents due to the very low pH, As, Sb and U removal by magnetite was studied by reacting with PG wastewater after raising and adjusting the pH at around 5.5, which has been observed as the minimum optimal value for their removal in the current study and in literature (**Missana et al., 2003; Singer et al., 2012; Verbinnen et al., 2013**). Indeed, U was fully removed from the PG wastewater solution, after only 30 min of reaction with magnetite, with no desorption following (**Fig. 3**). However, As and Sb sorption rates were low (**Fig. 3**; 22% and 13%, accordingly), similarly to the experiment on the synthesized water with U, As and Sb, despite the higher pH conditions, corroborating the antagonistic effect of high phosphate concentration present in the PG wastewater.

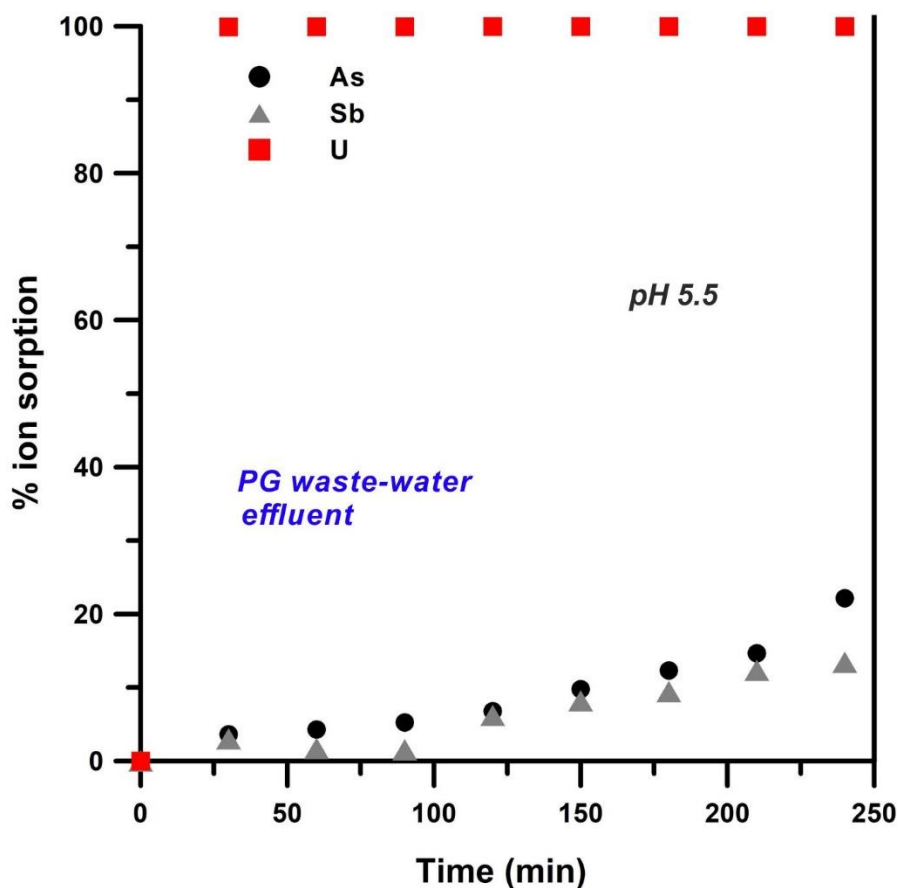


**Figure 3:** Sorption rate of As, Sb, and U through time of the PG waste-water effluents after adjusting the pH at 5.5.

### 3.5 NZVI oxidation

The production of  $\text{Fe}^{2+}$  and the pH increase following anaerobic corrosion of NZVI (Eq. 1) were investigated at very acidic conditions (pH ~ 2.5), mimicking those of the PG waste effluents. As shown in **Figure 4**, the initial concentration of NZVI added in the acidic solution had an effect in both pH and  $[\text{Fe}^{2+}]$  evolution through time. At  $[\text{NZVI}] = 0.1 \text{ g/L}$  the pH increase was very slow (**Fig. 4A**). It increased from 2.5 to 4 in 60 min and even after 240 min, the pH remained lower than pH 5. The respective production of ferrous iron was gradual, reaching ~1 mM in 60 min and ~1.3 mM in 240 min. At double NZVI concentration (0.2 g/L), the rise of the pH and the respective  $\text{Fe}^{2+}$  production were very fast (**Fig. 4B**). A pH value of 5.57 was reached already after 10 min, with 0.8 mM of dissolved  $\text{Fe}^{2+}$ , while at 1 h the pH was 8 with 1.5 mM of  $\text{Fe}^{2+}$  in solution. So, despite a large difference in final pH in the two experiments, the dissolved  $\text{Fe}^{2+}$  concentration was not significantly different.

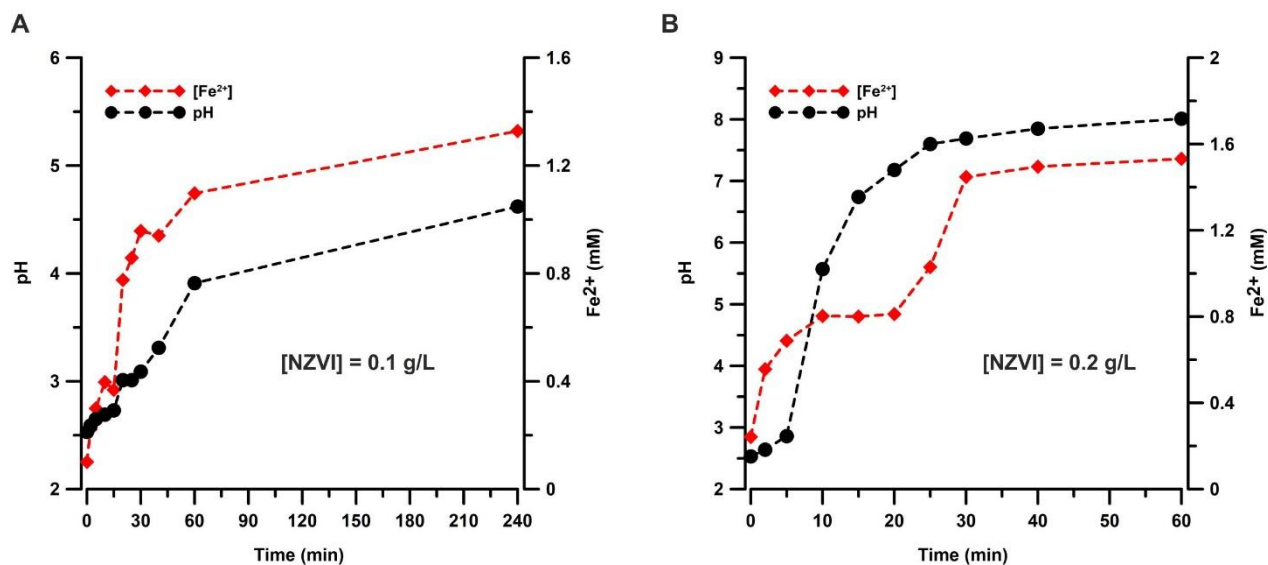


**Figure 4:** Behaviour of pH and [Fe<sup>2+</sup>] during NZVI oxidation at initial pH = 2.5. [NZVI] equals to 0.1 g/L (A), and 0.2 g/L (B).

### 3.6 Vivianite formation

The precipitates from the kinetic experiments were collected and analysed by XRD and SEM-EDS to observe the effect of saturation index and Fe/P molar ratio on the morphology and crystallinity of vivianite. At low [PO<sub>4</sub><sup>3-</sup>] (i.e. 1 and 5 mM), the precipitates were amorphous and thus, identification of vivianite by XRD was not feasible. At higher PO<sub>4</sub><sup>3-</sup> concentrations (10, 15 and 25 mM) vivianite formation could be clearly confirmed by XRD (**Fig. 5A**), and specifically for the highest ones (15 and 25 mM), at all Fe/P molar ratios (**e.g. Fig. 5B**). The results from the SEM-EDS analysis corroborate those from XRD, and showed that vivianite formation and morphology depended on [PO<sub>4</sub><sup>3-</sup>] concentration, and thus on the SI of the solution with respect to vivianite, and on the pH conditions (**Table 1**). At low [PO<sub>4</sub><sup>3-</sup>] (i.e. 5 mM), and SI < 8, vivianite was observed to be amorphous (**Fig. 6A**), with a Fe/PO<sub>4</sub><sup>3-</sup> equal to 50/50, and not 60/40, as is usually the case for vivianite, based on its structural formula (Fe<sub>3</sub>(PO<sub>4</sub>)<sub>2</sub>). On the other hand, for higher [PO<sub>4</sub><sup>3-</sup>], and for a SI > 8, vivianite appeared to form rod-shaped crystals (**Fig. 6C and D**), but also with a mixture of amorphous precipitates, due to the rapid drop of pH (since the solution is not buffered), and the drying processes that favoured the amorphous material over the crystalline. An exception was observed at the precipitates corresponding to [PO<sub>4</sub><sup>3-</sup>] = 10 mM and Fe/P = 1, where large vivianite crystals could be identified (**Fig. 6B**). This could be explained by the fact that, at relatively lower saturation indexes (Table 1) but over the threshold for formation

of crystalline vivianite (i.e., at  $[\text{PO}_4^{3-}] > 5\text{mM}$ ), the nucleation of crystalline vivianite may be relatively slower in comparison to a faster growth rate.

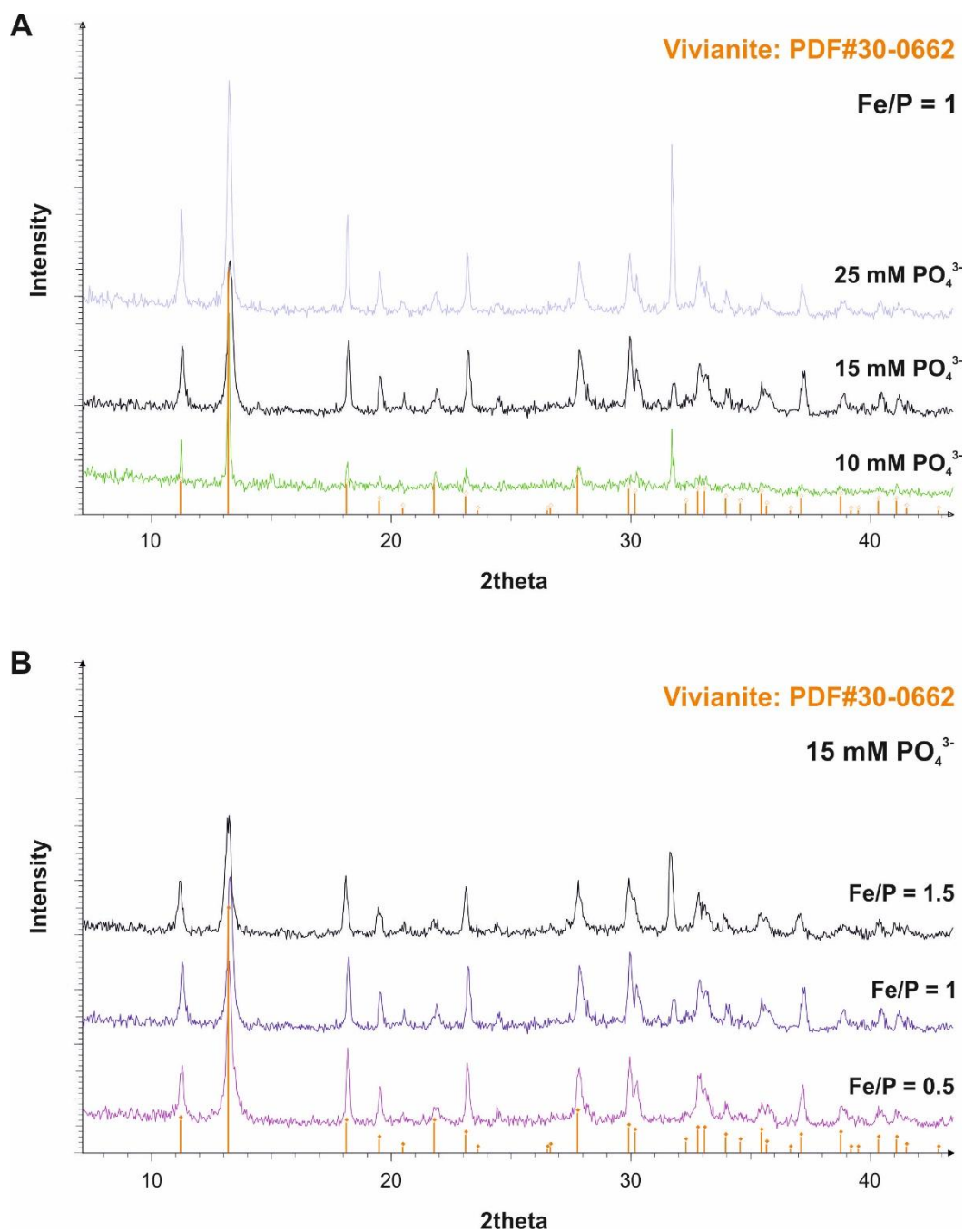


**Figure 5:** XRD patterns of precipitated material of the vivianite-formation experiments at **A)** different  $[\text{PO}_4^{3-}]$  at 1 Fe/P molar ratio, and **B)** at different Fe/P molar ratios at  $[\text{PO}_4^{3-}] = 15\text{mM}$ .

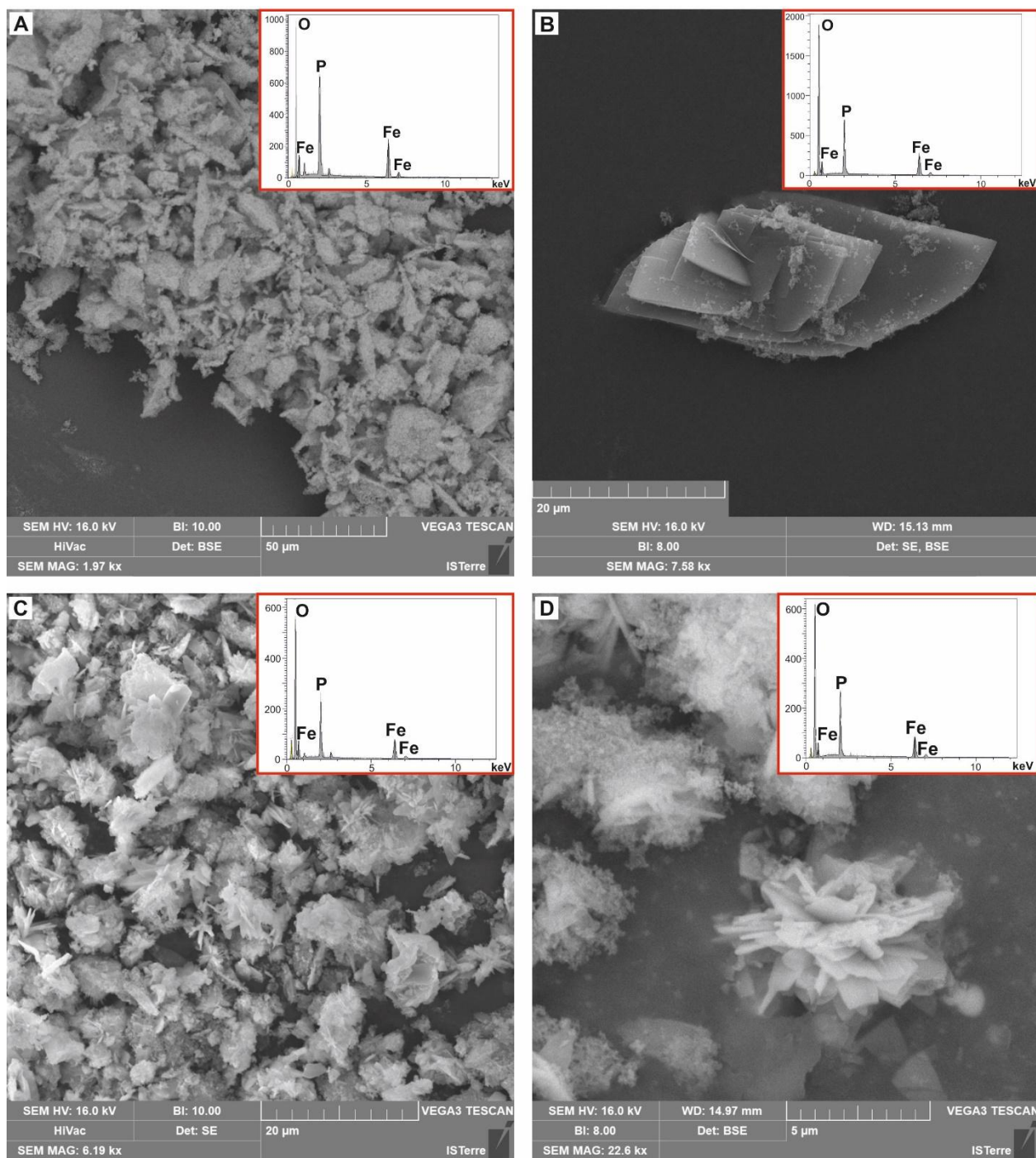
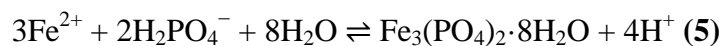
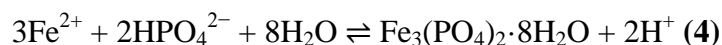


**Figure 6:** SEM images and the respective EDS spectra of vivianite formed at: **A)**  $[\text{PO}_4^{3-}] = 5 \text{ mM}$ , **B)**  $[\text{PO}_4^{3-}] = 10 \text{ mM}$ , **C)**  $[\text{PO}_4^{3-}] = 15 \text{ mM}$ , and **D)**  $[\text{PO}_4^{3-}] = 25 \text{ mM}$ , all at a molar Fe/P ratio = 1.

Various precipitation kinetic experiments were performed to explore the optimal parameters (pH, Fe/P ratio,  $[\text{PO}_4^{3-}]$ ) for the formation of vivianite in acidic conditions. The results of the experiments did not show important differences in the kinetics at different Fe/P molar ratios (**Table 1**); however, at Fe/P = 0.5 vivianite identification by XRD was limited, supported by SEM analysis showing amorphous material, due to the insufficient concentration of dissolved  $\text{Fe}^{2+}$ . Similar studies have shown that vivianite formation is more favoured at high Fe/P molar ratios, i.e. equal to 1.5, while excess of  $\text{Fe}^{2+}$  is undesirable, as it interferes with the purity of vivianite (**Cao et al., 2019**). The pH is also one of the driving parameters for vivianite precipitation as the phosphate species activity varies with pH. The fact that no buffer was used during the experiments led to a rapid drop of pH once the precipitation reaction started, according to **Eqs. (4) and (5)**, so no further vivianite precipitation was feasible (**Fig. 7**).



This explains the fact that no more phosphate was removed from solution already after up to 5 min (**Fig. 7**). The initial concentration of  $\text{PO}_4^{3-}$  played an important role for the reaction and it affected the pH conditions under which precipitation happens; the higher the  $[\text{PO}_4^{3-}]$ , the lowest the pH in which vivianite precipitation was feasible and the higher its removal % from solution. As such, up to 44%, 28%, and 17% removal of dissolved phosphate was achieved, when its initial concentrations were 25, 15, and 10 mM, respectively. On the contrary, the removal was limited for initial  $[\text{PO}_4^{3-}] = 5$  mM (**Table 1**).

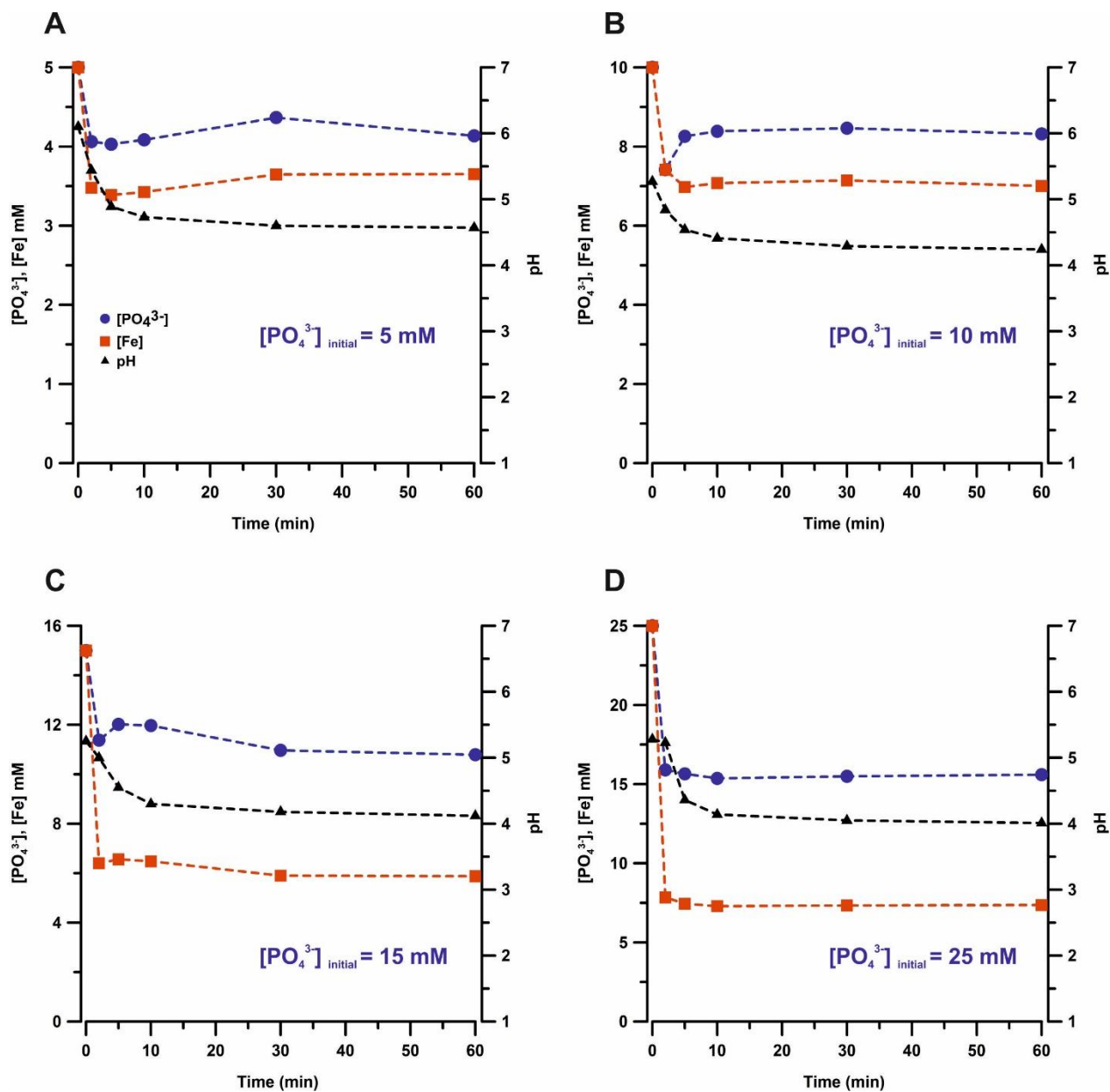


**Figure 7:**  $\text{PO}_4^{3-}$  and Fe concentrations (mM) during kinetic experiments of vivianite formation as a function of pH, at different initial  $[\text{PO}_4^{3-}]$ : **A)**  $[\text{PO}_4^{3-}] = 5 \text{ mM}$ , **B)**  $[\text{PO}_4^{3-}] = 10 \text{ mM}$ , **C)**  $[\text{PO}_4^{3-}] = 15 \text{ mM}$ , and **D)**  $[\text{PO}_4^{3-}] = 25 \text{ mM}$ , all at a molar Fe/P ratio = 1.

The same experiments were conducted under UV-Vis to follow the evolution of the absorbance of the solution, as a proxy for the kinetics of nucleation and precipitation. As shown in **Figure 8**, the induction time of vivianite nucleation could not be followed: the increase in absorbance occurs instantaneously after the mixing of the solutions, preventing a precise determination of the time needed for nucleation to occur. The results are presented in **Figure 8** as a function of the

$\text{PO}_4^{3-}$  concentration and the Fe/P ratio. At  $[\text{PO}_4^{3-}] = 5\text{mM}$  (**Fig. 8A**), and at  $[\text{PO}_4^{3-}] = 10\text{mM}$  and  $\text{Fe/P} = 0.5$  (**Fig. 8B**), which correspond to aqueous conditions of supersaturation with respect to vivianite ( $\text{SI} \sim 8$ ), the curves show a smooth logarithmic like evolution of the absorbance. On the contrary, for higher phosphate concentrations, the curves show both a sigmoidal behaviour continued by a logarithmic-like increase of the absorbance. We interpret the presence of two steps as a double precipitation mechanism, with the initial formation of one phase (probably an amorphous precipitate) and its subsequent recrystallization into vivianite. The absolute value of the absorbance is directly proportional to the initial phosphate concentration, which indicates a higher degree of precipitation, probably resulting from faster growth rates. The result of the experiment at  $[\text{PO}_4^{3-}] = 5\text{mM}$ , showing a single logarithmic evolution, is consistent with the initial formation of an initial amorphous precipitate. These results are consistent with the well-crystallized vivianite observed by SEM-EDS analyses when  $\text{SI} > 8$ , and the poorly crystalline material retrieved at the end of the experiments where  $\text{SI} < 8$ , which could not be identified by XRD. In all cases, the drop of pH following vivianite formation (expected from eq. 4) and the unbuffered pH conditions, was a decisive parameter for the presented results. As vivianite formation is pH dependent, and no buffer was used to keep pH stable and equal to a desiring value, vivianite formation stopped after pH dropped.

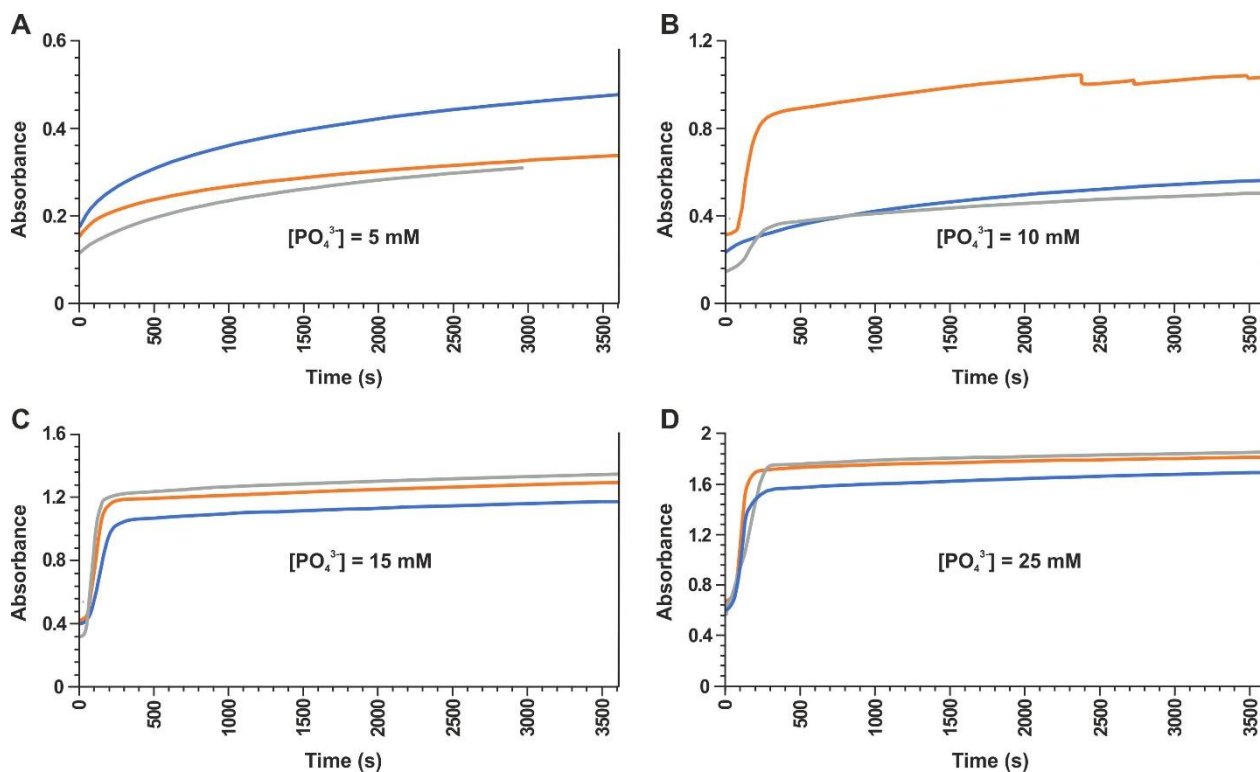


**Figure 8:** UV-Vis spectra following the nucleation of vivianite at: **A)**  $[\text{PO}_4^{3-}] = 5 \text{ mM}$ , **B)**  $[\text{PO}_4^{3-}] = 10 \text{ mM}$ , **C)**  $[\text{PO}_4^{3-}] = 15 \text{ mM}$ , and **D)**  $[\text{PO}_4^{3-}] = 25 \text{ mM}$ . Blue, orange and grey lines correspond to Fe/P molar ratios equal to 0.5, 1, and 1.5, respectively.

## 4. Discussion

### 4.1 PG treatment limiting factors: low pH and high phosphate

The most restrictive factor for the efficient removal of toxic pollutants from PG effluents is their extreme acidity that hinders the (co)precipitation/adsorption processes of these contaminants. To achieve optimal removal of the contaminants of interest (As, Sb, and U) from the PG leachates by magnetite, pH value around 5.5 needs to be reached. Common techniques used for pH increase prior to efficient treatment, include lime addition, and seawater mixing. According to **Papaslioti et al. (2018b)**, enormous amounts of seawater are needed to neutralise the effluents, and in order to reach a pH value of 5.5, the seawater to acidic leachate ratio is 50 to 100, thus four times lower than to reach pH 7 (**Fig. 9**). Thus, mixing with the local seawater is an efficient and cost-effective way to increase the pH of the PG effluents prior to their reaction with magnetite, but it has the drawback to dilute much the effluent and thus, to overdimension the facilities. Another promising mechanism to increase PG effluent pH is to treat it with (N)ZVI, which can be also used as a source of  $\text{Fe}^{2+}$  in order to precipitate vivianite, and thus to decrease phosphate concentration. In the current study, the anaerobic oxidation of NZVI (**Eq. 1**), triggered the pH increase in highly acidic solutions (**Figure 4**), showing a rapid efficiency in pH adjustment, while not diluting the effluent and not requiring large amounts of magnetite.

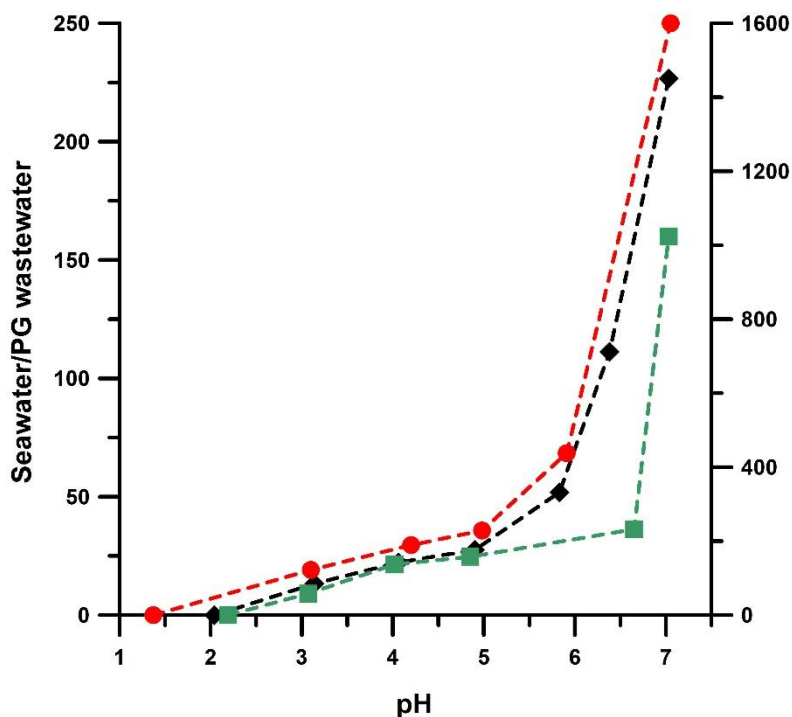


**Figure 9:** Mixing ratios of seawater to PG leachates as a function of pH. Each plot corresponds to different types of PG wastewater: the black diamonds to edge outflow water of an untreated PG area, the green squares to edge outflow water of a theoretically treated PG area, and the red circles to process water (the mixing ratios of the latter correspond to the values displayed in the right y axis). The figure is modified after Papaslioti et al. (2018b), where more details can be found on the different types of PG water and on the mixing ratios.

The presence of phosphate ions in contaminated leachates at high concentration is the second most limiting factor for the immobilisation of toxic elements (i.e. As and Sb), and as such, their removal from solution is crucial, e.g. via the formation of vivianite. The amount of ferrous iron and phosphate, their molar ratio, and the pH are the most important parameters controlling the nucleation and precipitation pathways of vivianite. The optimal pH range for vivianite precipitation is 7 to 9, while at pH <5, almost all  $\text{Fe}^{2+}$  and  $\text{PO}_4^{3-}$  ions remain in solution (Liu et al.; 2018; Cao et al., 2019), though an increased initial  $\text{PO}_4^{3-}$  concentration favors a wider pH range where vivianite formation occurs (i.e. pH 4 to 11), due to the higher ionic strength that favours the competition with  $\text{OH}^-$  ions and as such, meeting the  $K_{sp}$  of vivianite (März et al., 2018; Cao et al., 2019). These later observations show that the formation of vivianite is feasible in PG effluent conditions (high concentrations of  $\text{PO}_4^{3-}$  and pH < 6 the targeted pH value for immobilisation of contaminants of interest). This was confirmed by our kinetic experiments

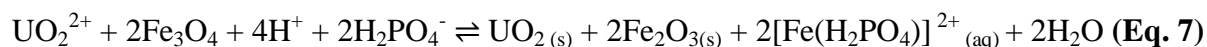
which showed that vivianite formation is feasible in a pH range of 4.5 to 6, especially in the presence of high  $\text{PO}_4^{3-}$  concentrations (**Table 1; Fig.7**).

#### 4.2 Reductive immobilisation of $\text{U}^{6+}$

Uranium immobilisation on magnetite at pH 5 and 7 confirms previous XPS, XAS, and Mössbauer spectroscopy-based studies on the occurrence of  $\text{U}^{6+}$  reductive precipitation to  $\text{UO}_2(\text{s})$ , a  $10^5$  less soluble phase than U(VI) salts, with the formation of a possible surface  $\text{U}^{5+}$  intermediate reaction step (**Scott et al., 2005; Aamrani et al., 2007; Latta et al., 2011; Pan et al., 2020**). The recent **Pan et al. (2020)** study, shows that at neutral pH conditions,  $\text{UO}_2$  nanowires are formed that ultimately collapse into nanoclusters. The reduction occurs most likely at the surface of (nano)magnetite and is driven by the electron transfer between Fe and U. In our sorption experiments, the very fast release by magnetite of  $\text{Fe}^{2+}(\text{aq})$  at pH 5 was stopped after  $\text{U}^{6+}$  addition and sorption reaction (**Figs. 1A and C**), indicating a two-step reaction: first a cation exchange of  $\text{Fe}^{2+}$  and  $\text{UO}_2^{2+}$ , at the magnetite surface. Second, a 2-electron transfer from magnetite to U, with maghemite formation being coupled to  $\text{UO}_2^{2+}(\text{aq})$  reduction to  $\text{UO}_2(\text{s})$ , according to **Eq. 6**:



Despite the suspension becoming more acidic according to **Eq. 6**, aqueous Fe concentration remained constant, as  $\text{Fe}_2\text{O}_3$  has a low solubility at pH 5. However, the mechanism that is suggested for the behaviour of Fe and U in our experiments cannot be efficiently shown due to the relatively low concentration of U compared to the instability of the magnetite. During the phosphate-rich sorption experiments, the decrease of magnetite dissolution from  $t = 140$  to 210 min observed at pH 5 (**Fig. 1B**) was due to phosphate adsorption, vivianite surface precipitation, and/or decrease of surface charge that would decrease the magnetite dissolution kinetics. A simultaneous removal of  $\text{UO}_2^{2+}$  and the  $\text{Fe}^{2+}$  is also, observed in presence of phosphate (**Figs. 1B and 1D**). The layer of a Fe-phosphate mineral (e.g. vivianite) potentially formed on the surface of magnetite, would block the mineral dissolution and passivating it. However, total Fe concentration in solution increased afterwards, which means that aqueous Fe phosphate complexation was favoured (i.e. **Eq. 7**).



If  $\text{Fe}^{3+}$  was released, it could complex  $\text{PO}_4^{3-}$  ions as an aqueous complex species (i.e.  $\text{FePO}_4^0$ ), while dissolution of magnetite, potentially releases ferrous and ferric iron ions, which can complex phosphate ions. Magnetite Fe oxidation coupled to U reduction will control the kinetics of it (**Figs. 1B and D**). In general, the high concentration of phosphate present during the reaction of magnetite with U did not hinder its efficient removal from solution, as shown in **figure 1D**. However, we observed an opposite behaviour at pH 7 and 5 compared to experiments without phosphate (**Fig. 1C vs Fig. 1D; Table S1**). Under high phosphate concentration the reaction is faster at pH 5, whereas without phosphate it is faster at pH 7. At neutral pH, phosphate hinders the formation of  $\text{UO}_2$  and promotes that of monomeric  $\text{U}^{4+}$ , such as  $\text{U}_3(\text{PO}_4)_4^0$  precipitate/complex (**Veeramani et al., 2011**). More specifically, the monomeric  $\text{U}^{4+}$  mostly likely occurs as surface complex species on vivianite surfaces, and appears to be coordinated to phosphate rather than to  $\text{Fe}^{2+}$ . On the contrary,  $\text{U}^{6+}$  presents a lower reduction compared to that in phosphate-free suspensions, since adsorbed phosphate blocks further U adsorption and slows down the transfer of electrons from  $\text{Fe}^{2+}$  to  $\text{U}^{6+}$ , corroborating the lower removal during the present experiments on phosphate-rich suspensions (**Fig. 1D**). Also, phosphate complexing  $\text{UO}_2^{2+}$  in solution, e.g. as  $(\text{UO}_2\text{HPO}_4)^0$ , being the only slow decomplexation leading to reductive precipitation could be considered for the lower U removal from solution when phosphate is present. At pH 5, similarly to the  $\text{PO}_4^{3-}$ -free experiments, the driving processes that control the solubility of U are first, the reduction of  $\text{U}^{6+}$  to  $\text{U}^{4+}$ , and then its precipitation, i.e. as  $(\text{UO}_2)_3(\text{PO}_4)_2$  (s), at the surface of magnetite or elsewhere. The behaviour of U and  $\text{PO}_4^{3-}$  is a matter of kinetic of decomplexation of uranyl; uranyl is neutral, so it is quickly adsorbed. When  $\text{PO}_4^{3-}$  adsorption occurs, the surface of magnetite becomes negatively charged, favouring electrostatically U adsorption, which is fast (**Fig. 1D**). At pH 2, different phosphate complexes formed, so we should have  $\text{H}_3\text{PO}_4$  compared to before. So, at least half of the phosphate should be as  $\text{H}_3\text{PO}_4$  and still half as  $\text{H}_2\text{PO}_4$ , indicating an elevated presence of protons, which explains why the formation of  $\text{H}_3\text{PO}_4$  outcompetes that of  $\text{Fe}^{3+}$ . Uranium removal is not minimal when phosphate adsorption occurs, in contrast with the phosphate-free solution, due to screening of the positive surface charge, and thus, favouring the  $\text{UO}_2^{2+}$  adsorption by electrostatics and further U reduction.

### 4.3 Competitive sorption of As and Sb

Reduction of  $\text{As}^{5+}$  and  $\text{Sb}^{5+}$  to their trivalent form is feasible by magnetite, forming a stable sorption complex on its surface, under a pH and time dependent adsorbance, substituting the position occupied by tetrahedral  $\text{Fe}^{3+}$  (Auffan et al., 2008; Kirsch et al., 2008; Wang et al., 2008; Mittal et al., 2013). Indeed, both reduced  $\text{As}(\text{OH})_3^0$  and  $\text{Sb}(\text{OH})_3^0$  species are sorbed through a loss of  $3\text{H}^+$  and a tridentate surface. The limitation of As and Sb uptake in the phosphate rich waters studied in the present research is attributed to the presence of phosphate anion competing with As and Sb on magnetite (e.g. Chowdhury and Yanful, 2010) for (co)precipitation and/or adsorption processes or on Fe minerals in contaminated waters of different pH values (Zhang et al., 2004; Papaslioti et al., 2018b; Millán-Becerro et al., 2019; Papaslioti et al., 2020). Phosphate anion has the same sorption mechanism as the two oxyanions of interest and the significantly higher  $\text{PO}_4^{3-}$  concentration present in the phosphogypsum wastewaters compared to that of As and Sb inhibits their immobilisation. However, based on the results of the present study, after rising the pH at a value close to 5.5 and removing the phosphate via vivianite precipitation, As and Sb could be efficiently removed from the PG effluents by reductive precipitation on magnetite. Under these conditions,  $\text{As}^{5+}$  and  $\text{Sb}^{5+}$  are efficiently reduced to their trivalent form, that can form a stable surface tridentate complex on magnetite.

## **5. Conclusions: A novel treatment technology for acidic, phosphate rich waters**

Phosphogypsum is a highly contaminated waste that threatens the environmental welfare worldwide through pollutant leaching from PG stacks. In addition, the acidity and high phosphate concentration in those effluents are hindering the removal of most inorganic contaminants. In this study, we examine magnetite as an immobilisation agent for As, Sb, and U redox sensitive contaminants contained in PG waste effluents through adsorption and/or reduction processes. We use magnetite derived from recycling waste of the steel industry in compliance with 'green' chemistry technology, that is advantageous for large scale applications. We show that U is efficiently removed from both phosphate free and phosphate rich solutions at pH 5-7. However, phosphate anions compete with As and Sb oxyanions for magnetite sorption sites and they are efficiently immobilised only at phosphate-free conditions. We address the acidity and phosphate obstacles by using (nano)zero-valent-iron as a source of ferrous iron and pH increase with the aim to remove phosphate from contaminated waters via vivianite precipitation prior to reaction with magnetite. In this study, we, therefore, set the basis for an alternative remediation technique for contaminated, acidic, phosphate-rich waters. In the case of PG, the wastewater leaching from

the stacks will first, enter a reactor where (N)ZVI will raise the pH at around 5.5 (optimal conditions for As, Sb, and U reduction and adsorption) and enough  $\text{Fe}^{2+}$  will be produced for vivianite formation, thus for the removal of phosphate ions to a level where competition with As and Sb oxyanions for magnetite surface sites would be low. The resulted solution will pass into a following reactor, where vivianite will be formed and precipitate. The resulted solution will then, pass to a third reactor of the treatment set-up, to react with the magnetite from the recycling industry with the aim to immobilise the contaminants of interest, and finally result in a decontaminated water. Further studies for optimisation of the suggested remediation strategy are necessary, for upscaling and framing the flux of the solution during the different steps, residence times in each reactor, and necessary amounts of (N)ZVI and magnetite to be used according to the needs.

### **Credit authorship contribution statement**

**Evgenia-Maria Papaslioti:** Conceptualization; Data curation; Formal analysis; Funding acquisition; Investigation; Methodology; Project administration; Resources; Supervision; Validation; Visualization; Writing - original draft; Writing - review & editing. **Philippe Le Bouteiller:** Formal analysis; Investigation; Validation; Writing - review & editing. **Hugo Carreira:** Data curation; Formal analysis; Investigation; Visualization; Writing - original draft. **Alejandro Fernandez-Martinez:** Investigation; Methodology; Supervision; Validation; Writing - review & editing. **Laurent Charlet:** Conceptualization; Funding acquisition; Investigation; Methodology; Project administration; Resources; Supervision; Validation; Writing - review & editing.

### **Declaration of Competing Interest**

The authors declare that they have no known competing financial interests or personal relationships that could have appeared to influence the work reported in this paper.

### **Acknowledgements**

This work was supported by the European Union's Horizon 2020 research and innovation programme under the Marie Skłodowska-Curie grant agreement No. 892570. We thank Dr. Nathaniel Findling for the XRD and SEM-EDS, and Dr. Valérie Magnin for the BET analyses, respectively. We are grateful to Dr. Delphine Tisserand and Dr. Simona Denti for their assistance

during laboratory and analytical work. All experiments and analyses were performed within the analytical chemistry platform of ISTerre (OSUG France). We also, acknowledge Dr. Nicolas Menguy from IMPMC, Sorbonne University (Paris) for the Transmission Electron Microscopy (TEM), and Selected Area Electron Diffraction (SEAD) analyses. We also, thank the Environmental Mineralogy and Geochemistry Group from the University of Huelva (Spain), for our useful discussions, and for providing waste-water sample for our research.

## References

Abril, J. M., García-Tenorio, R., Periañez, R., Enamorado, S. M., Andreu, L., & Delgado, A. (2009). Occupational dosimetric assessment (inhalation pathway) from the application of phosphogypsum in agriculture in South West Spain. *Journal of Environmental Radioactivity*, *100*(1), 29-34.

Anderson, L. C., & Bruland, K. W. (1991). Biogeochemistry of arsenic in natural waters: the importance of methylated species. *Environmental science & technology*, *25*(3), 420-427.

Almeelbi, T., & Bezbaruah, A. (2012). Aqueous phosphate removal using nanoscale zero-valent iron. In *Nanotechnology for Sustainable Development* (pp. 197-210). Springer, Cham.

Bae, S., & Hanna, K. (2015). Reactivity of nanoscale zero-valent iron in unbuffered systems: effect of pH and Fe (II) dissolution. *Environmental science & technology*, *49*(17), 10536-10543.

Boreiko, C. J., & Rossman, T. G. (2020). Antimony and its compounds: Health impacts related to pulmonary toxicity, cancer, and genotoxicity. *Toxicology and Applied Pharmacology*, *403*, 115156.

Brunet, F., Crouzet C., & Goffe, B. (2017). Method for producing nanomagnetite. (France, Patent No WO2017211845A1). Centre National De La Recherche Scientifique. <https://patents.google.com/patent/WO2017211845A1/en>

Cánovas, C. R., Macías, F., Pérez-López, R., Basallote, M. D., & Millán-Becerro, R. (2018). Valorization of wastes from the fertilizer industry: current status and future trends. *Journal of Cleaner Production*, *174*, 678-690.

Cao, J., Wu, Y., Zhao, J., Jin, S., Aleem, M., Zhang, Q., ... & Luo, J. (2019). Phosphorus recovery as vivianite from waste activated sludge via optimizing iron source and pH value during anaerobic fermentation. *Bioresource technology*, *293*, 122088.

Charlet, L., & Polya, D. A. (2006). Arsenic in shallow, reducing groundwaters in southern Asia: an environmental health disaster. *Elements*, *2*(2), 91-96.

Choe, S., Chang, Y. Y., Hwang, K. Y., & Khim, J. (2000). Kinetics of reductive denitrification by nanoscale zero-valent iron. *Chemosphere*, *41*(8), 1307-1311.

Chowdhury, S. R., & Yanful, E. K. (2010). Arsenic and chromium removal by mixed magnetite–maghemite nanoparticles and the effect of phosphate on removal. *Journal of environmental management*, *91*(11), 2238-2247.

Crane, R. A., Dickinson, M., Popescu, I. C., & Scott, T. B. (2011). Magnetite and zero-valent iron nanoparticles for the remediation of uranium contaminated environmental water. *Water research*, *45*(9), 2931-2942.

Crouzet, C., Brunet, F., Recham, N., Auzende, A. L., Findling, N., Magnin, V., ... & Goffé, B. (2017). Hydrothermal steel slag valorization—Part II: Hydrogen and nano-magnetite production. *Frontiers in Earth Science*, *5*, 86.

El Aamrani, S., Giménez, J., Rovira, M., Seco, F., Grive, M., Bruno, J., ... & De Pablo, J. (2007). A spectroscopic study of uranium (VI) interaction with magnetite. *Applied surface science*, *253*(21), 8794-8797.

Filella, M., Belzile, N., & Chen, Y. W. (2002). Antimony in the environment: a review focused on natural waters: II. Relevant solution chemistry. *Earth-Science Reviews*, *59*(1-4), 265-285.

Gorski, C. A., Nurmi, J. T., Tratnyek, P. G., Hofstetter, T. B., & Scherer, M. M. (2010). Redox behavior of magnetite: Implications for contaminant reduction. *Environmental science & technology*, *44*(1), 55-60.

He, Y. T., & Traina, S. J. (2005). Cr (VI) reduction and immobilization by magnetite under alkaline pH conditions: the role of passivation. *Environmental science & technology*, *39*(12), 4499-4504.

Iconaru, S. L., Guégan, R., Popa, C. L., Motelica-Heino, M., Ciobanu, C. S., & Predoi, D. (2016). Magnetite (Fe<sub>3</sub>O<sub>4</sub>) nanoparticles as adsorbents for As and Cu removal. *Applied clay science*, *134*, 128-135.

Kanel, S. R., Manning, B., Charlet, L., & Choi, H. (2005). Removal of arsenic (III) from groundwater by nanoscale zero-valent iron. *Environmental science & technology*, *39*(5), 1291-1298.

Kirsch, R., Scheinost, A. C., Rossberg, A., Banerjee, D., & Charlet, L. (2008). Reduction of antimony by nano-particulate magnetite and mackinawite. *Mineralogical Magazine*, *72*(1), 185-189.

Latta, D. E., Gorski, C. A., Boyanov, M. I., O'Loughlin, E. J., Kemner, K. M., & Scherer, M. M. (2012). Influence of magnetite stoichiometry on UVI reduction. *Environmental Science & Technology*, *46*(2), 778-786.

Liu, J., Cheng, X., Qi, X., Li, N., Tian, J., Qiu, B., ... & Qu, D. (2018). Recovery of phosphate from aqueous solutions via vivianite crystallization: thermodynamics and influence of pH. *Chemical Engineering Journal*, *349*, 37-46.

Liu, Y., & Wang, J. (2019). Reduction of nitrate by zero valent iron (ZVI)-based materials: a review. *Science of the Total Environment*, *671*, 388-403.

Lottermoser, B. G. (2010). Introduction to mine wastes. In *Mine wastes* (pp. 1-41). Springer, Berlin, Heidelberg.

Lu, Y., Liu, H., Feng, W., Xu, Y., & Chen, X. (2021). A new and efficient approach for phosphorus recovery from wastewater in the form of vivianite mediated by iron-reducing bacteria. *Journal of Water Process Engineering*, *42*, 102200.

Macías, F., Cánovas, C. R., Cruz-Hernández, P., Carrero, S., Asta, M. P., Nieto, J. M., & Pérez-López, R. (2017). An anomalous metal-rich phosphogypsum: Characterization and classification according to international regulations. *Journal of Hazardous Materials*, *331*, 99-108.

Martinez, M., Giménez, J., De Pablo, J., Rovira, M., & Duro, L. (2006). Sorption of selenium (IV) and selenium (VI) onto magnetite. *Applied Surface Science*, *252*(10), 3767-3773.

- Millán-Becerro, R., Pérez-López, R., Macías, F., Cánovas, C. R., Papaslioti, E. M., & Basallote, M. D. (2019). Assessment of metals mobility during the alkaline treatment of highly acid phosphogypsum leachates. *Science of The Total Environment*, 660, 395-405.
- März, C., Riedinger, N., Sena, C., Kasten, S., 2018. Phosphorus dynamics around the sulphate-methane transition in continental margin sediments: authigenic apatite and Fe(II) phosphates. *Mar. Geol.* 404, 84–96.
- Miot, J., Benzerara, K., Morin, G., Bernard, S., Beyssac, O., Larquet, E., ... & Guyot, F. (2009). Transformation of vivianite by anaerobic nitrate-reducing iron-oxidizing bacteria. *Geobiology*, 7(3), 373-384.
- Missana, T., Alonso, U., Scheinost, A. C., Granizo, N., & García-Gutiérrez, M. (2009). Selenite retention by nanocrystalline magnetite: Role of adsorption, reduction and dissolution/co-precipitation processes. *Geochimica et Cosmochimica Acta*, 73(20), 6205-6217.
- Mittal, V. K., Bera, S., Narasimhan, S. V., & Velmurugan, S. (2013). Adsorption behavior of antimony (III) oxyanions on magnetite surface in aqueous organic acid environment. *Applied surface science*, 266, 272-279.
- Pan, Z., Bártoová, B., LaGrange, T., Butorin, S. M., Hyatt, N. C., Stennett, M. C., ... & Bernier-Latmani, R. (2020). Nanoscale mechanism of UO<sub>2</sub> formation through uranium reduction by magnetite. *Nature communications*, 11(1), 1-12.
- Parsons, C.T., Couture, R.M., Omoregie, E.O., Bardelli, F., Greneche, J.M., Roman-Ross, G., Charlet, L., 2013. The impact of oscillating redox conditions: arsenic immobilisation in contaminated calcareous floodplain soils. *Environ. Pollut.* 178, 254-263.
- Papaslioti, E. M. **a**, Pérez-López, R., Parviainen, A., Macías, F., Delgado-Huertas, A., Garrido, C. J., ... & Nieto, J. M. (2018a). Stable isotope insights into the weathering processes of a phosphogypsum disposal area. *Water research*, 140, 344-353.
- Papaslioti, E. M. **b**, Pérez-López, R., Parviainen, A., Sarmiento, A. M., Nieto, J. M., Marchesi, C., ... & Garrido, C. J. (2018b). Effects of seawater mixing on the mobility of trace elements in acid phosphogypsum leachates. *Marine pollution bulletin*, 127, 695-703.

Papaslioti, E. M., Pérez-López, R., Parviainen, A., Phan, V. T., Marchesi, C., Fernandez-Martinez, A., ... & Charlet, L. (2020). Effects of redox oscillations on the phosphogypsum waste in an estuarine salt-marsh system. *Chemosphere*, *242*, 125174.

Pérez-López, R., Macías, F., Cánovas, C. R., Sarmiento, A. M., & Pérez-Moreno, S. M. (2016). Pollutant flows from a phosphogypsum disposal area to an estuarine environment: an insight from geochemical signatures. *Science of the Total Environment*, *553*, 42-51.

Poulain, A., Fernandez-Martinez, A., Greneche, J. M., Prieur, D., Scheinost, A. C., Menguy, N., ... & Charlet, L. (2022). Selenium Nanowire Formation by Reacting Selenate with Magnetite. *Environmental Science & Technology*.

Schwertmann, U. T. R. M., & Taylor, R. M. (1989). Iron oxides. *Minerals in soil environments*, *1*, 379-438.

Scott, T. B., Allen, G. C., Heard, P. J., & Randell, M. G. (2005). Reduction of U (VI) to U (IV) on the surface of magnetite. *Geochimica et Cosmochimica Acta*, *69*(24), 5639-5646.

Singer, D. M., Chatman, S. M., Ilton, E. S., Rosso, K. M., Banfield, J. F., & Waychunas, G. A. (2012). Identification of simultaneous U (VI) sorption complexes and U (IV) nanoprecipitates on the magnetite (111) surface. *Environmental Science & Technology*, *46*(7), 3811-3820.

Tayibi, H., Choura, M., López, F. A., Alguacil, F. J., & López-Delgado, A. (2009). Environmental impact and management of phosphogypsum. *Journal of environmental management*, *90*(8), 2377-2386.

Tseng, W. P., Chu, H., How, S. W., Fong, J. M., Lin, C. S., & Yeh, S. H. U. (1968). Prevalence of skin cancer in an endemic area of chronic arsenicism in Taiwan. *Journal of the national Cancer institute*, *40*(3), 453-463.

Veeramani, H., Alessi, D. S., Suvorova, E. I., Lezama-Pacheco, J. S., Stubbs, J. E., Sharp, J. O., ... & Bernier-Latmani, R. (2011). Products of abiotic U (VI) reduction by biogenic magnetite and vivianite. *Geochimica et Cosmochimica Acta*, *75*(9), 2512-2528.

Verbinnen, B., Block, C., Lievens, P., Van Brecht, A., & Vandecasteele, C. (2013). Simultaneous removal of molybdenum, antimony and selenium oxyanions from wastewater by adsorption on supported magnetite. *Waste and Biomass Valorization*, *4*(3), 635-645.

Wang, C. B., & Zhang, W. X. (1997). Synthesizing nanoscale iron particles for rapid and complete dechlorination of TCE and PCBs. *Environmental science & technology*, 31(7), 2154-2156.

Wilson, S. C., Lockwood, P. V., Ashley, P. M., & Tighe, M. (2010). The chemistry and behaviour of antimony in the soil environment with comparisons to arsenic: a critical review. *Environmental pollution*, 158(5), 1169-1181.

Wu, Y., Luo, J., Zhang, Q., Aleem, M., Fang, F., Xue, Z., & Cao, J. (2019). Potentials and challenges of phosphorus recovery as vivianite from wastewater: A review. *Chemosphere*, 226, 246-258.

Yang, J., Liu, W., Zhang, L., & Xiao, B. (2009). Preparation of load-bearing building materials from autoclaved phosphogypsum. *Construction and Building Materials*, 23(2), 687-693.

Yean, S., Cong, L., Yavuz, C. T., Mayo, J. T., Yu, W. W., Kan, A. T., ... & Tomson, M. B. (2005). Effect of magnetite particle size on adsorption and desorption of arsenite and arsenate. *Journal of Materials Research*, 20(12), 3255-3264.

Zhang, W. X. (2003). Nano scale iron particles for environmental remediation: an overview. *J. Nanopart. Res.*, 5, 323-332.

Zhang, M., Wang, Y., Zhao, D., & Pan, G. (2010). Immobilization of arsenic in soils by stabilized nanoscale zero-valent iron, iron sulfide (FeS), and magnetite (Fe<sub>3</sub>O<sub>4</sub>) particles. *Chinese Science Bulletin*, 55(4), 365-372.

Zhang, W., Singh, P., Paling, E., & Delides, S. (2004). Arsenic removal from contaminated water by natural iron ores. *Minerals engineering*, 17(4), 517-524.